Fabrication of exchange-coupled α-Fe/$L1_0$-FePd nanocomposite isolated particles

Junichi Kawamura, Kazuhisa Sato,[a] and Yoshihiko Hirotsu
The Institute of Scientific and Industrial Research (ISIR), Osaka University, 8-1 Mihogaoka, Ibaraki, Osaka 567-0047, Japan

(Received 23 February 2004; accepted 18 June 2004)

Oriented nanocomposite particles of α-Fe and ordered $L1_0$-FePd have been fabricated by electron-beam deposition and successive postdeposition annealing at temperatures higher than 773 K. High-resolution transmission electron microscopy, nanobeam electron diffraction, and nanobeam elemental analysis indicated that two regions composed of α-Fe and $L1_0$-FePd coexisted in each nanoparticle separated by a diffuse boundary. Magnetic hysteresis measurements using a superconducting quantum interference device magnetometer showed a gradual increase in the saturation magnetization with increasing volume ratio of the α-Fe region, whereas the coercivity decreased with the volume of α-Fe. There were no obvious steps in each magnetization curve. These results indicated the existence of an exchange coupling between the α-Fe and $L1_0$-FePd crystallites connected coherently with each other within the nanoparticles. The effects of the α-Fe region size on hard magnetic properties are also discussed. © *2004 American Institute of Physics*. [DOI: 10.1063/1.1782963]

I. INTRODUCTION

Ferromagnetic nanoparticles have attracted a great deal of interest for scientific and industrial uses due to their characteristic properties of superparamagnetism, rotation magnetization of single-domain particles, and application of these phenomena to magnetic sensors or storage media. Particles smaller than their magnetic-domain wall size become "single-magnetic-domain particles" with unidirectional orientation of the magnetic moment, where the magnetization process of the particles is carried by rotation magnetization. For such small particles, ideally, we can obtain a maximum coercivity value as large as the anisotropy field.[1] One of the most active topics of research in this field is the fabrication of films with ultrahigh-density magnetic nanoparticles for future ultrahigh-density magnetic recording.[2,3] However, the magnetic moment of a nanoparticle is easily perturbed by thermal agitation, which finally results in the appearance of superparamagnetism. The critical particle size of the transition from ferromagnetism to superparamagnetism of the magnetic nanoparticles due to the thermal agitation can be discussed using the following relation under the constant K_u value, $K_uV \sim 25\ k_BT$, where K_u is the uniaxial magnetocrystalline anisotropy constant, V is the critical volume of the magnetic particle, k_B is the Boltzmann constant, and T is the temperature.[4–6] This relation indicates that the large K_u value is necessary for the ferromagnetic nanoparticles to overcome the thermal agitation under a small V value. In recent years, a great deal of attention has been paid to the fabrication of the $L1_0$-FePt thin films[7,8] or $L1_0$-FePt nanoparticles[9,10] with hard magnetic properties. This is because $L1_0$-FePt has a large K_u value (6.6×10^6 J/m^3) (Ref. 11) compared to CoPtCr-based recording materials.[12] For the isolated single-domain $L1_0$-FePt nanoparticles, room-temperature coercivities as large as 40 ~ 70 kOe[13,14] have been reported. However, the saturation magnetization (M_s) of the $L1_0$-FePt phase (1140 emu/cm^3) (Ref. 11) is much smaller than that of the pure α-Fe (1710 emu/cm^3).[15]

To increase the M_s of hard magnetic materials, we referred to the previous studies of permanent magnets that took advantage of the exchange coupling between the soft magnetic phase with a high M_s and the hard magnetic phase with a large K_u. Among these magnets, called "exchange-spring magnets" or "nanocomposite magnets," a maximum energy product as high as 24 MG Oe was obtained for the α-Fe/$Nd_2Fe_{14}B$ nanocomposite prepared by melt spinning.[16] Zeng *et al.*[17,18] reported the formation of the exchange-coupled Fe_3Pt/FePt films using a chemical technique called "self-assembly of magnetic nanoparticles." In contrast to the Fe–Pt alloy, there is a eutectoid reaction at 878 K in the equilibrium phase diagram of the Fe–Pd alloy[19] at the composition of Fe-46 at.%Pd. The coexistence of the two phases, i.e., soft magnetic α-Fe and hard magnetic $L1_0$-FePd with a large K_u value (2.6×10^6 J/m^3),[20] can be realized on cooling from the eutectoid temperature to room temperature. A two-phase mixture is obtained in a wide composition range between the pure Fe and the 48.5 at.%Pd. In addition, the noble-metal content can be reduced effectively by choosing the Fe-rich composition of the Fe–Pd alloy. Due to the small magnetocrystalline anisotropy constant of α-Fe (4.7×10^4 J/m^3) (Ref. 21) and its high M_s value, it is presumed that the two-phase mixture behaves as an exchange-spring magnet. Despite these technological advantages of the α-Fe/$L1_0$-FePd nanocomposite alloy, there have been no previous studies especially with regard to nanoparticles.

In the present study, we fabricated the exchange-coupled α-Fe/$L1_0$-FePd nanoparticles with a mutual fixed orientation

[a]Electronic mail: sato@sanken.osaka-u.ac.jp

and good isolation. The results regarding nanostructures, morphology, and magnetic properties in relation to the Fe composition are presented in this article.

II. EXPERIMENT

Specimen preparation was performed by successive deposition of Pd and Fe using an electron-beam evaporation apparatus with a base pressure of approximately 3×10^{-7} Pa. Pure Pd, Fe, and Al_2O_3 crystals were used as evaporation sources, and NaCl(001) crystals cleaved in air were supplied as substrates. A quartz thickness monitor attached to the evaporation chamber was used to estimate the average thickness of the deposited layer. In this process, we took advantage of the overgrowth of Fe onto the Pd "seed" nanoparticles, which were grown epitaxially on the cleaved NaCl(001) substrates with a substrate temperature of 623 K.[22] After deposition, an amorphous (a-)Al_2O_3 film was further deposited at a substrate temperature of about 573 K to protect the particles from oxidation and also to stabilize the particles in the separated condition. The average thicknesses for Pd, Fe, and Al_2O_3 were 1, $2\sim5$, and 10 nm, respectively. By changing the average deposition thickness of Fe, we fabricated three kinds of specimens with different alloy compositions. The energy dispersive x-ray spectroscopy (EDS) indicated that the mean compositions of these specimens were Fe-43 at.%Pd (for a specimen with an average Fe thickness of 2 nm), Fe-33 at.%Pd (Fe thickness of 3 nm), and Fe-25 at.%Pd (Fe thickness of 5 nm). Heat treatments of the as-deposited specimens for the formation of the ordered FePd were performed in a high-vacuum furnace ($<8\times10^{-5}$ Pa) at 873 K for 3.6 ks. The heating and cooling rates were 5 and 10 K/min, respectively. The as-deposited and the annealed films were removed from the NaCl substrate by immersing the substrate into distilled water and were mounted onto copper grids for transmission electron microscopy (TEM) using 200 kV (JEOL, JEM-2010) and 300 kV (JEOL, JEM-3000F) electron microscopes. The TEM images and electron diffraction patterns were recorded on imaging plates (IP, Fuji Film, FDL-UR-V), and the electron intensities were processed as digital data. *In situ* observations during annealing were also made in the 200 kV electron microscope with a specimen-heating stage. Magnetic properties were measured using a superconducting quantum interference device (SQUID) magnetometer (Quantum Design, MPMS-5S) over the temperature range between 10 and 300 K.

III. RESULTS AND DISCUSSION

Average film thicknesses, alloy compositions, and mean particle sizes of the specimens are listed in Table I. The specimens with the initial average Fe thickness of 2, 3, and 5 nm were designated as specimens A, B, and C, respectively. Here, we present the results of the structural characterization mainly for specimen C. The TEM images and the corresponding selected area electron diffraction (SAED) patterns for the as-deposited specimen (a) and also for the specimen annealed at 873 K for 3.6 ks (b) are shown in Fig. 1. In the SAED pattern in Fig. 1(a), reflections from α-Fe, fcc Pd, and a weak halo pattern from a-Al_2O_3 are seen, whereas no superlattice reflections from the $L1_0$-FePd compound are detected. Successive deposition of Pd and Fe onto the heated substrate resulted in the formation of isolated particles of Fe/Pd nanocomplex with a mutual fixed orientation. The orientation relationship was as follows: $\langle011\rangle_{NaCl}//\langle011\rangle_{Pd}$, $\{100\}_{NaCl}//\{100\}_{Pd}$, $\langle100\rangle_{Fe}//\langle100\rangle_{Pd}$, and $\{011\}_{Fe}//\{010\}_{Pd}$. In the image in Fig. 1(a), dark- and gray-contrast regions can be seen in each nanoparticle. The dark- and gray-contrast regions, due mainly to absorption, were considered to be of fcc Pd and α-Fe, respectively. Strongly dark-contrast regions are also observed in some particles, which are due to a diffraction effect. Postdeposition annealing led to the formation of the tetragonal-ordered phase with the $L1_0$-type ordered structure. In the SAED pattern shown in Fig. 1(b), in addition to the 200 Fe reflection, 001 and 110 superlattice reflections from the $L1_0$-FePd are visible, implying the coexistence of α-Fe and $L1_0$-FePd in the specimen. The TEM image shown in Fig. 1 clearly indicates the isolation of the nanoparticles. The particle-size distribution followed a log-normal-type distribution function. The mean particle size of the as-deposited specimen was 21 nm with a standard deviation of $\ln\sigma=0.22$, where as that for the annealed specimen

TABLE I. Alloy compositions and mean-particle sizes of the as-deposited ($D_{as\text{-}depo}$) and annealed specimens (D_{anneal}) with different average Fe thickness.

Specimen	Average thickness	Alloy composition (at.%Pd)	$D_{as\text{-}depo}$ (nm)	D_{anneal} (nm)
A	Fe(2 nm)/Pd(1 nm)	Fe-43	12	12
B	Fe(3 nm)/Pd(1 nm)	Fe-33	15	14
C	Fe(5 nm)/Pd(1 nm)	Fe-25	21	21

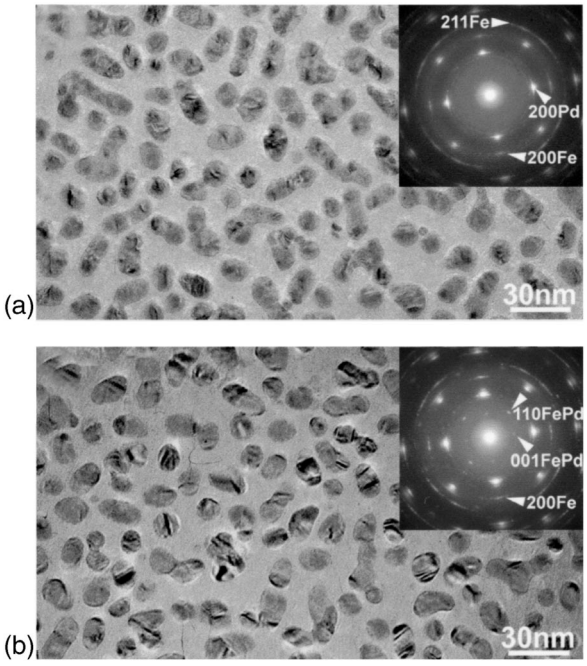

FIG. 1. TEM images and corresponding SAED patterns of the as-deposited (a) and annealed (b) specimen C. The TEM images indicated the formation of the isolated nanoparticles.

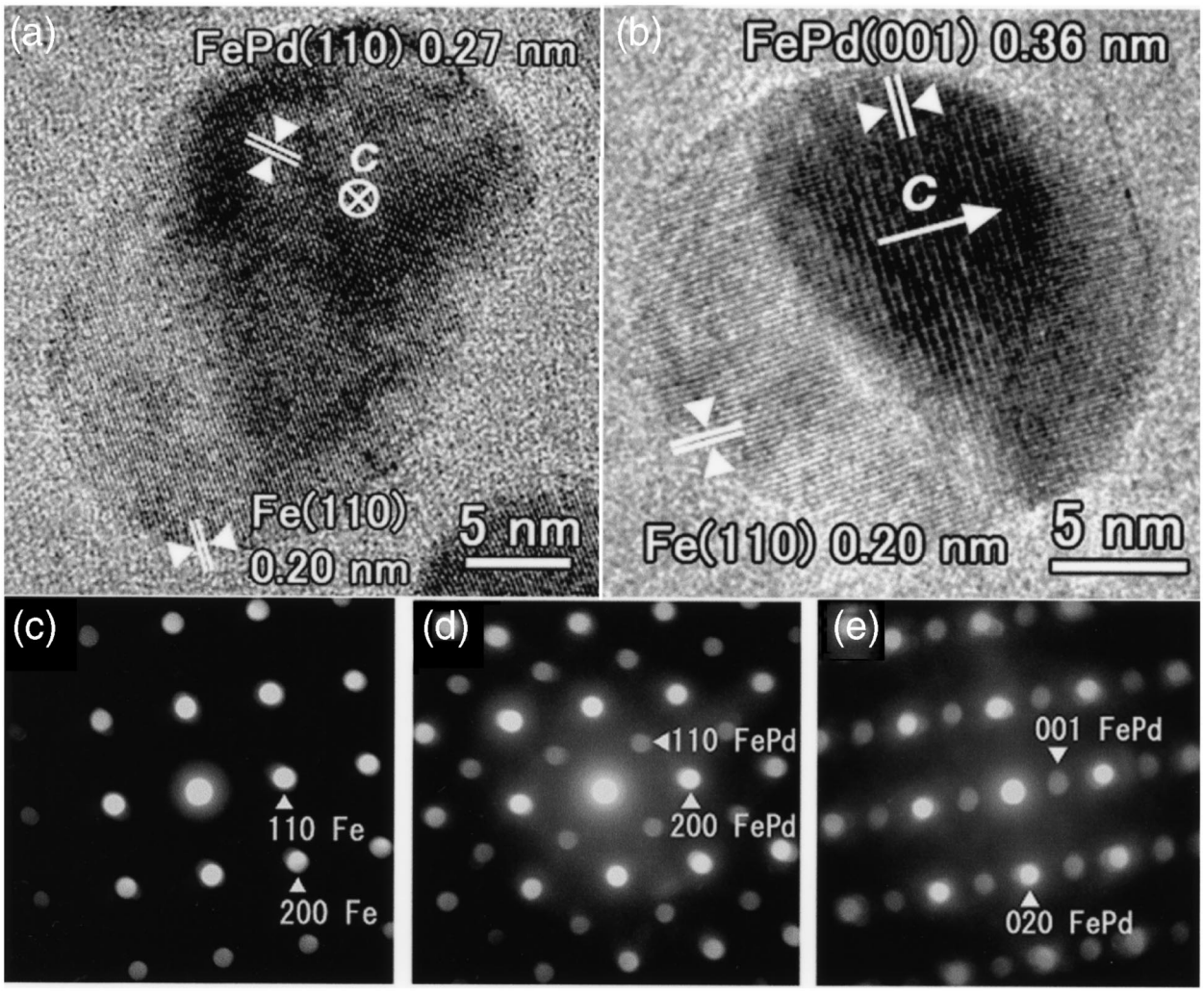

FIG. 2. HRTEM images and NBD patterns of annealed specimen C. The NBD patterns were obtained by applying a nanoprobe of approximately 3 nm. The α-Fe region and the $L1_0$-FePd region with the c axis oriented perpendicular (a) and parallel (b) to the film plane can be seen. The NBD patterns correspond to the local regions in the nanoparticles with α-Fe (c) and $L1_0$-FePd of the c axis perpendicular (d) and parallel (e) to the film plane.

was 21 nm with a standard deviation of $\ln \sigma = 0.23$, indicating that no obvious coalescence of nanoparticles occurred during the annealing. This also indicates that both the alloying and the atomic ordering reactions proceeded within each Fe/Pd nanocomplex particle during the postdeposition annealing.

Local structural analyses of the nanoparticles were performed using the high-resolution TEM (HRTEM) and the nanobeam electron diffraction (NBD). Figures 2(a) and 2(b) show examples of the HRTEM images of the FePd nanoparticles in specimen C annealed at 873 K. In both of the images, gray- and dark-contrast regions can be seen in each nanoparticle. From the lattice-fringe spacing, the dark-contrast region was found to be of $L1_0$-FePd. On the other hand, for the gray contrast region, it was not easy to differentiate between the lattice fringe of the α-Fe(110) with the [001] beam incidence from that of the disordered FePd(200) with the [001] beam incidence because of the epitaxial orientation relation between α-Fe and Pd (or FePd). However, according to the Fe–Pd equilibrium phase diagram,[19] the disordered Fe–Pd phase with the fcc structure cannot exist at 873 K in the specimens used here with compositions of 25 $\sim$43 at.% Pd. Therefore, the gray-contrast region was judged to be of α-Fe. This was further confirmed by the results of the NBD and the compositional analysis using a nanoprobe. In Fig. 2(a), a region of $L1_0$-FePd with the c axis oriented perpendicular to the film plane can be seen, which was coherently connected to a gray-contrast region of α-Fe, both of which were in epitaxial orientation relation with the NaCl(100) substrate. Lattice fringes with spacings of 0.20 and 0.27 nm are clearly seen, corresponding to the (110) plane spacings of α-Fe and $L1_0$-FePd, respectively. In addition, a particle consisting of an $L1_0$-FePd region with the c axis oriented parallel to the film plane and an α-Fe region were also seen [Fig. 2(b)]. During the TEM observation, we found that a larger number of particles had their c axes oriented normal to the film plane as compared with those oriented parallel to the film plane. The preferential c-axis orientations of the $L1_0$-FePd regions perpendicular to the film plane were also confirmed by the SAED pattern [Fig. 1(b)], as the intensity of the 110 superlattice reflection was much stronger than that of the 001. These results were consistent with our previous study on single-crystalline $L1_0$-FePd nanoparticles.[23]

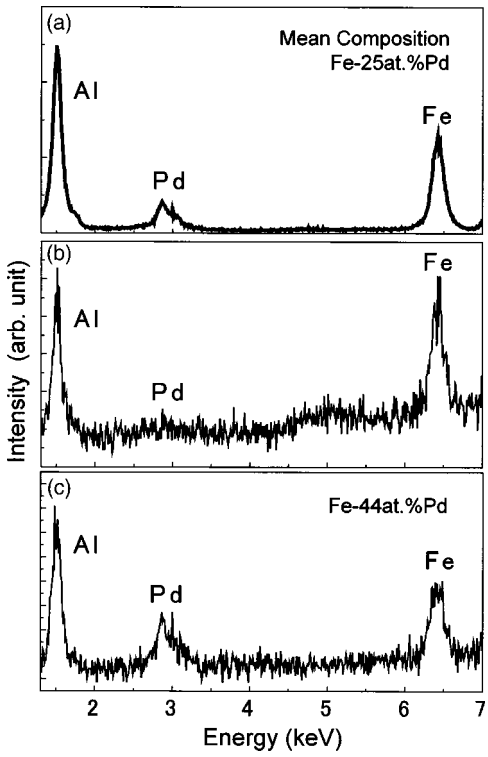

FIG. 3. EDS spectra obtained from the wide region (1.25 μm in diameter) (a), α-Fe region (b), and $L1_0$-FePd region (c) of the annealed specimen C. The size of the electron nanoprobe was approximately 3 nm. The Fe counts for (a), (b), and (c) were 1300, 100, and 100, respectively.

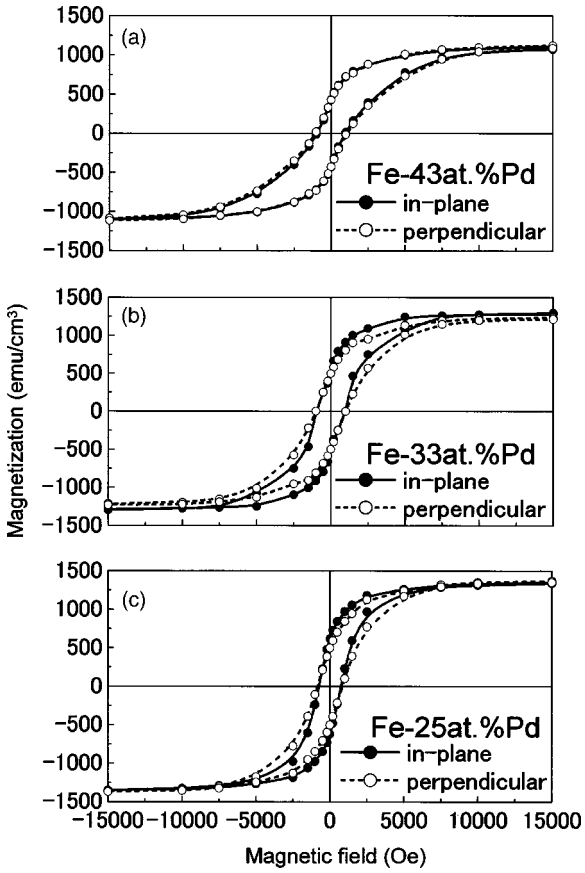

FIG. 4. Magnetization curves of the annealed specimen A (a), specimen B (b), and specimen C (c). Magnetization curves were measured at 300 K with the external field both parallel (solid circles) and perpendicular (open circles) to the film plane.

The NBD patterns also explained the coexistence of α-Fe and $L1_0$-FePd in each nanoparticle. In the NBD experiments, an electron beam was focused on the local regions of various particles. The size of the nanoprobe used was estimated to be approximately 3 nm, which was measured from the full width at half maximum of the nanoprobe intensity profile recorded on IP. The NBD patterns shown in Figs. 2(c)–2(e) are from the local regions of α-Fe [Fig. 2(a)], $L1_0$-FePd [Fig. 2(a): beam $\perp$ c axis], and $L1_0$-FePd [Fig. 2(b): beam // c axis], respectively. This two-phase composite structure in nanoparticles was also seen after annealing specimens A and B. In addition, the size of the α-Fe region increased in the order of specimens A, B, and C on annealing. The observed two-phase nanocomposite was considered to consist of a partly alloyed $L1_0$-FePd phase and a residual α-Fe after alloying and atomic ordering reactions. It has been reported for the bulk Fe-Pd alloy that the phase separation of α-Fe and $L1_0$-FePd from the disordered Fe-Pd alloy obtained after water quenching from 1273 K requires a long annealing time of more than 360 ks at 873 K.[24,25] These results suggest that it is not easy to obtain the α-Fe/$L1_0$-FePd nanocomposite structure using a eutectoid reaction.

Figure 3 shows the intensity profiles of the EDS spectra analyzed from a wide area [1.25 μmϕ: Fig. 3(a)] and local areas [3 nm ϕ: Figs. 3(b) and 3(c)] for the annealed specimen as shown in Figs. 1 and 2. The EDS spectra in Fig. 3(a) resulted in an alloy composition of Fe-25 at.%Pd, which corresponded to the mean composition of specimen C. From a gray-contrast region, as seen in Fig. 2(a) or 2(b), we obtained the EDS spectrum shown in Fig. 3(b), where the sharp Fe-K peak can be seen clearly, whereas the Pd-L peak is very weak. In contrast, an almost equiatomic alloy composition was obtained from a dark-contrast region, as seen in Fig. 3(c). These represent further evidence of the coexistence of the Fe and FePd regions in a single particle.

Figure 4 shows the magnetization curves of the specimens with different alloy compositions after annealing at 873 K. Magnetization curves were measured at 300 K with the external field both parallel (solid circles) and perpendicular (open circles) to the film plane. Coercivity values around 1 kOe were obtained from the annealed specimens. These results corresponded to the formation of the $L1_0$-FePd ordered phase with a large K_u value. The coercivity (H_c) measured with the external field perpendicular to the film plane was slightly larger than that with the in-plane field. This was explained by the preferential c-axis orientation of $L1_0$-FePd perpendicular to the film plane observed by the TEM. The shapes of the magnetization curves indicate that the changes of the magnetization were smooth with the magnetic field, and no obvious steps were observed in the magnetization processes for all the specimens, although the specimens consisted of a nanocomposite with magnetically hard $L1_0$-FePd and soft α-Fe. These characteristic magnetization processes, like that of a single-phase hard magnet, indicated the existence of an effective exchange-magnetic coupling between the hard and the soft phases in the present specimens. Theo-

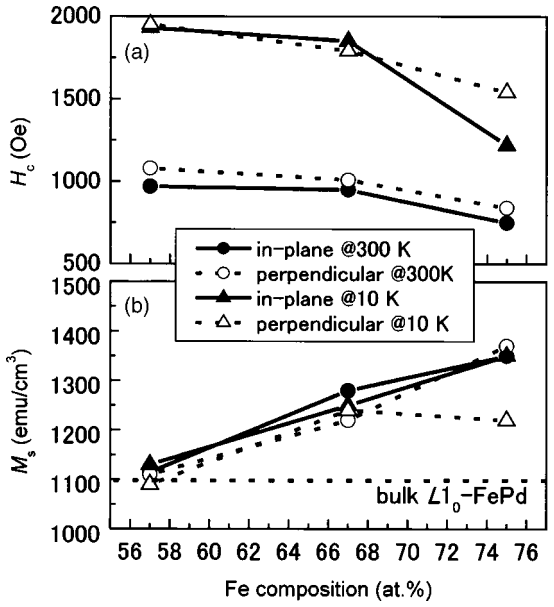

FIG. 5. The changes in the values of coercivity (H_c) (a) and the saturation magnetization (M_s) (b) as a function of the Fe composition for the 873 K annealed specimen. These magnetic properties were measured at 300 K and 10 K, respectively.

retical calculations have indicated that the dimension of the soft phase should be less than twice the domain-wall thickness in the hard phase for the purpose of the effective exchange coupling between them.[26,27] From the HRTEM observation of the α-Fe/$L1_0$-FePd nanoparticles in the annealed specimen C, we estimated the size of the α-Fe regions connected to the $L1_0$-FePd regions. The size was defined as the distance from the α-Fe/$L1_0$-FePd interface to the end of the α-Fe region. The mean size of the α-Fe regions was 7 nm and the maximum size was 15 nm. In the $L1_0$-FePd phase, the magnetic-domain wall thickness is about 7.5 nm,[11] so exchange coupling between α-Fe and $L1_0$-FePd can be fully realized according to the theoretical calculations. From the relation between the size of the α-Fe regions and the increase in magnetization, it is reasonable to consider that the effective exchange coupling between the soft α-Fe and the hard $L1_0$-FePd regions, similar to the exchange-spring or nanocomposite magnets, has been realized.

We also measured the magnetization curves at 10 K. Figure 5 shows the obtained magnetic properties H_c [Fig. 5(a)] and M_s [Fig. 5(b)] as a function of the Fe composition. The values of H_c were around 1 and 2 kOe at 300 and 10 K, respectively, and decreased with increases in the Fe composition. The values of M_s measured at 300 and 10 K were comparable, and both were higher than that of a single $L1_0$-FePd phase (1100 emu/cm^3) (Ref. 20) and increased monotonically with the Fe composition toward the value of a single $L1_0$-FePd phase. The maximum M_s was 1370 emu/cm^3 at 25 at.%Pd (specimen C), which was 25% higher than the value of a single $L1_0$-FePd phase.

IV. CONCLUSION

We fabricated the exchange-coupled α-Fe/$L1_0$-FePd nanocomposite particles by annealing the Fe/Pd nanocomplex particles at temperatures higher than 773 K. A mutual fixed orientation and coherent interface was found between α-Fe and $L1_0$-FePd due to epitaxial growth the HRTEM, NBD, and nano-EDS analysis indicated the coexistence of these two-phase regions in every nanoparticle. A gradual increase in the saturation magnetization with increasing Fe content was observed by magnetic measurements, whereas coercivity was decreased with Fe composition. No obvious steps were found in each magnetization curve. These results indicated the existence of the exchange coupling between α-Fe and $L1_0$-FePd crystalline regions connected with each other within the nanoparticles. The size of α-Fe in the specimen fabricated in the present study was thought to be the ideal size for the effective exchange coupling between the α-Fe and the $L1_0$-FePd phase. Determination of the long-range order parameter of the $L1_0$-FePd phase is the next step to clarify in more detail the relation between the nanostructure and the hard magnetic properties of the present specimen.

ACKNOWLEDGMENTS

The authors wish to thank Professor T. Kawai and Dr. H. Tanaka of ISIR, Osaka University, for their help with the SQUID measurement. This study was supported by the Center of Excellence (COE) program at ISIR, Osaka University, Grants-in-Aid for Scientific Research (Grant Nos. 14205094, 13555189, and 15760490), and Special Coordination Funds for Promoting Science and Technology on "Nanohetero metallic materials" from the Ministry of Education, Culture, Sports, Science, and Technology, Japan.

[1] C. Kittel, Rev. Mod. Phys. **21**, 541 (1949).
[2] I. Chado, S. Padovani, F. Scheurer, and J. P. Bucher, Appl. Surf. Sci. **164**, 42 (2000).
[3] A. Sugawara and M. R. Scheinfein, Phys. Rev. B **56**, R8499 (1997).
[4] L. Néel, Ann. Geophys. (C.N.R.S.) **5**, 99 (1949).
[5] C. P. Bean and J. D. Livingston, J. Appl. Phys. **30**, 120S (1959).
[6] D. J. Sellmyer, M. Yu, and R. D. Kirby, Nanostruct. Mater. **12**, 1021 (1999).
[7] M. R. Visokay and R. Sinclair, Appl. Phys. Lett. **66**, 1692 (1995).
[8] T. Shima, T. Morigushi, S. Mitani, and K. Takanashi, Appl. Phys. Lett. **80**, 288 (2002).
[9] M. Watanabe, T. Matsumoto, D. H. Ping, and K. Hono, Appl. Phys. Lett. **76**, 3971 (2000).
[10] S. Sun, C. B. Murray, D. Weller, L. Folks, and A. Moser, Science **287**, 1989 (2000).
[11] T. Klemmer, D. Hoydick, H. Okumura, B. Zhang, and W. A. Soffa, Scr. Metall. Mater. **33**, 1793 (1995).
[12] Y. Kubota, L. Folks, and E. E. Marinero, J. Appl. Phys. **84**, 6202 (1998).
[13] H. Shima, K. Takahashi, Y. K. Takahashi, K. Hono, G. Q. Li, and S. Ishio, J. Magn. Magn. Mater. **226**, 171 (2003).
[14] S. Okamoto, O. Kitakami, N. Kikuchi, T. Miyazaki, and Y. Shimada, Phys. Rev. B **67**, 094422 (2003).
[15] R. M. Bozorth, *Ferromagnetism* (D. Van Nostrand Co., Princeton, NJ, 1951) p. 870.
[16] X. Y. Zhang, Y. Guan, L. Yang, and J. W. Zhang, Appl. Phys. Lett. **79**, 2426 (2001).
[17] H. Zeng, J. Li, J. P. Liu, Z. L. Wang, and S. Sun, Nature (London) **420**, 395 (2002).
[18] J. Li, Z. L. Wang, H. Zeng, S. Sun, and J. P. Liu, Appl. Phys. Lett. **82**, 3743 (2003).
[19] T. B. Massalski, H. Okamoto, P. R. Subramanian, and L. Kacprzak, *Binary Alloy Phase Diagrams*, 2nd ed. (ASM International, Meterials Park, Ohio, 1990).
[20] A. Kussmann and K. Müller, Z. Angew. Phys. **17**, 509 (1964).
[21] H. Gengnagel and U. Hofmann, Phys. Status Solidi **29**, 91 (1968).

[22]B. Bian, K. Sato, Y. Hirotsu, and A. Makino, Appl. Phys. Lett. **75**, 3686 (1999).
[23]K. Sato and Y. Hirotsu, J. Appl. Phys. **93**, 6291 (2003).
[24]K. Watanabe, Trans. Jpn. Inst. Met. **24**, 144 (1983).
[25]H. Masumoto and K. Watanabe, Trans. Jpn. Inst. Met. **24**, 139 (1983).
[26]T. Schrefl, H. Kronmuller, and J. Fidler, J. Magn. Magn. Mater. **127**, L273 (1993).
[27]R. Skomski and J. M. D. Coey, Phys. Rev. B **48**, 015812 (1993).